INTERNATIONAL JOURNAL OF INTEGRATED ENGINEERING
ISSN: 2229-838X e-ISSN: 2600-7916

IJIE

Vol. 17 No. 9 (2025) 274-284
https://publisher.uthm.edu.my/ojs/index.php/jamea

Investigation on the Deposition of Conductive Ink on Multiple Substrates with Different Substrate Surface Energy and Ink Surface Tension Properties

Loo Yuen Hern[1], Rd. Khairilhijra Khirotdin[1]*, Nurhafizzah Hassan[1]

[1] *Faculty of Mechanical and Manufacturing Engineering,*
Universiti Tun Hussein Onn Malaysia, 86400 Parit Raja, Batu Pahat, Johor, MALAYSIA

*Corresponding Author: khairil@uthm.edu.my
DOI: https://doi.org/10.30880/ijie.2025.17.09.018

Article Info

Received: 11 March 2025
Accepted: 10 October 2025
Available online: 31 December 2025

Keywords

Conductive ink, mathematical model, syringe deposition system, substrate surface energy, ink surface tension

Abstract

Conductive ink is a transformative material that enables the printing of electronic circuits on a variety of substrates, revolutionizing the field of printed electronics. This study addresses the limitation of existing mathematical models for conductive ink deposition, which primarily assume ink deposition solely on generic substrates and printing on the fly, thus lacking adaptability for diverse applications. The objective is to integrate substrate surface energy and ink surface tension into mathematical model thus improve the precision of ink track width estimation. Employing a syringe deposition system, data analysis was conducted to develop an improved mathematical model that predicts ink deposition on various substrates while establishing optimal printing parameters. Experimental results indicated significant discrepancies in line widths, with initial measurements exceeding 2 mm and percentage errors surpassing 150%. By incorporating SSE, the improved model achieved line widths between 0.72 mm and 0.92 mm, significantly reducing the maximum error to 15.82%. The findings emphasize the crucial influence of substrate surface energy and ink surface tension on ink spreading and adhesion, particularly on substrates with varying porosity and absorbency.

1. Introduction

Conductive ink is a versatile material containing electrically conductive particles dispersed within a liquid medium and has revolutionized the field of printed electronics [1]. Its unique properties enable the printing of electronic circuits and components on various substrates, ranging from flexible plastics to rigid ceramics, revolutionizing traditional manufacturing processes. Its composition typically comprises of conductive particles suspended in a solvent or binder [2-3], allowing for easy deposition onto various substrates through printing techniques such as syringe, ink-jet, screen printing [4], or flexography has led to advancements in rapid prototyping, mass customization, and the creation of intricate, lightweight electronic devices. This ink finds extensive applications across diverse industries such as flexible circuits, RFID tags, smart labels, cell phone antennas, electrochemical sensors and energy harvesting [2,5], while in wearable technology, it facilitates the creation of smart textiles, biosensors, and flexible displays due to its compatibility with soft and stretchable materials [6]. The automotive sector benefits from conductive ink are printing sensors, antennas, and heating elements directly onto automotive interiors and exteriors [7]. Furthermore, conductive ink is integral to energy storage and generation, enabling the production of printed batteries, super-capacitors, and solar cells [8-9]. This versatile material offers numerous advantages, including flexibility, cost effectiveness, rapid prototyping capabilities, and customization options to meet specific application requirements. Despite its widespread use,

challenges such as improving conductivity and stability, reducing the cost of materials, addressing environmental concerns, and integrating with emerging technologies remain areas of active research and development [10]. Nonetheless, conductive ink continues to fuel innovation, driving advancements in electronic manufacturing and paving the way for novel applications in various sectors. A syringe deposition system, which uses a pressure-controlled syringe equipped with a micro-sized needle, enables the precise printing of conductive ink patterns in both 2D and 3D on a variety of substrates. This high-precision fluid dispensing device undergoes numerical analysis to develop a dynamic model that predicts conductive ink placement across different surfaces. Given the numerous printing parameters involved, however, the model's initial outputs offer only general estimation of ink deposition. Printed electronics encompass various methods, including ink-jet printing, screen printing, and offset printing, to create electronic devices on diverse substrates. With the rising demand for flexible displays, antennas, sensors, and compact electronic devices, printed electronics are increasingly pivotal. Syringe deposition systems, which precisely dispense liquid material, have applications in manufacturing, research, and medical procedures. Achieving the desired ink tracks involves control over key variables such as printing speed, pressure, ink viscosity, thickness, and nozzle tip size, as demonstrated by a previous mathematical model [11]. Based on fluid dynamics, this model provides theoretical values for the track width and height of printed patterns, assuming minimal dimensional change at the nozzle tip as the solvent evaporates. Forces acting at the tip include the driving pressure (P), polymer weight within the syringe, solvent vapor pressure, ST (γ), and dynamic friction, resulting in a multi-variable system with numerous possible solutions [11].

The previous mathematical model for the deposition of conductive ink underwent thorough validation through extensive experimental work and analysis [11-12]. However, this meticulous validation process highlighted a noteworthy limitation of the existing model, which primarily assumes ink deposition solely on generic substrates and printing on the fly. Given the ever-expanding spectrum of available substrates and the increasingly diverse range of applications within the dynamic field of printed electronics, there emerges a compelling imperative to enhance the model's comprehensiveness and adaptability. Specifically, the pressing need arises for the incorporation of substrate surface energy (SSE) as a variable, as its profound impact on the resulting physical properties of printed ink tracks has been empirically established [13]. Additionally, an ink's physical and chemical properties particularly ink surface tension (ST) significantly influence its drop formation, printability and wetting capability and could be adjusted to optimize its printing performance [14]. Given the range of substrates and applications, a more robust model should integrate SSE and ST to accurately capture these factors' effects on ink track properties during printing [15]. Therefore, this study aims to improve the predictive mathematical model for the deposition of conductive ink on multiple substrates by adding different SSE and ST properties and verify its accuracy through experimental investigations of conductive ink deposition.

In the mathematical modeling of conductive ink deposition, SSE plays a crucial role in predicting deposition outcomes and optimizing printing processes. SSE significantly influences wetting behavior, ink spreading, adhesion, and the quality of printed features [16-17]. High SSE encourage favorable wetting, promoting uniform ink spreading and well-defined patterns. Conversely, low SSE can hinder ink wetting, resulting in incomplete coverage and irregular patterns [18]. The adhesion between the ink and the substrate, directly affected by SSE, is essential for the durability and reliability of printed features [19]. Stronger interactions on high SSE substrates enhance adhesion, while poor adhesion on low energy substrates can lead to detachment or delamination. Additionally, SSE affects print quality by influencing the resolution and sharpness of printed features on different substrates, as well as their electrical performance [20]. Optimizing SSE allows for sharper, more precise patterns and ensures continuous ink pathways, which are critical for achieving consistent conductivity in printed electronics [21]. In essence, understanding and controlling SSE is essential for optimizing conductive ink deposition processes and achieving consistent, high-quality results in printed electronics applications. ST is equally vital in conductive ink deposition, governing droplet formation, spreading dynamics, and wetting behavior during printing [22-24]. Lower ST facilitates broader droplet spreading, enhancing feature placement accuracy and resolution, while higher ST restricts spreading, resulting in narrower lines. This balance between ST and SSE shapes wetting behavior and ensures optimal adhesion, allowing for high-quality patterning. ST also affects ink droplet trajectory from the printing nozzle, impacting the consistency and quality of the deposited features [25]. It influences conductivity, as conductive inks generally exhibit improved conductivity on substrates with larger ST [26]. Additionally, surface pre-treatment methods on low-energy substrates can improve printability and performance, while ink wettability, impacted by ST, determines ink-droplet dynamics and deposition morphology [19]. In effect, ST acts as both a conductor and a sculptor in conductive ink deposition, guiding droplet formation and enhancing the precision and reliability of printed electronic features. Incorporating SSE and ST into mathematical models allows for a more comprehensive understanding of the complex interactions between ink, substrate, and printing environment.

Int. Journal of Integrated Engineering Vol. 17 No. 9 (2025) p. 274-284

2. Material and Methods

2.1 Ink and Substrates

In this study, a silver-epoxy conductive ink (Model AG806), shown in Fig. 1(a), was selected for its superior electrical conductivity and oxidative stability. To ensure smooth conductive ink deposition, the ink viscosity was precisely adjusted to 2.4 Pa·s using toluene as a diluent. The viscosity measurements were conducted using a vibro-viscometer machine, illustrated in Fig. 1(b). Nine substrates with distinct SSE characteristics were selected for evaluation and categorized into three groups: low, medium, and high SSE, based on their SSE values. Each substrate was cut to a standardized size of 25.4 x 76.2 mm and cleaned in an ultrasonic bath to eliminate any surface contaminants that could impact measurement accuracy. Contact angle measurements were conducted using the VCA-Optima machine, shown in Fig. 1(c), to ensure precise SSE data. The SSE values and contact angles for each substrate are summarized in Table 3.

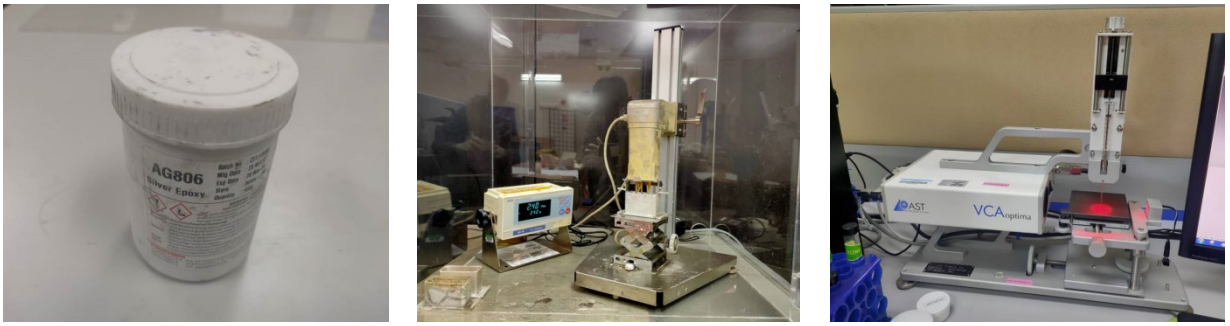

(a) **(b)** **(c)**

Fig. 1 *(a) Silver conductive ink (b) Vibro-viscometer; (c) VCA-Optima machine*

2.2 Model

In a prior study, researchers explored the width and thickness of printed patterns using a sophisticated model based on the original wetting framework [11]. The study recognized the inherent complexity of dynamic wetting systems as an essential asset for accurate predictions. To facilitate these predictions, Eq. (1) was developed as the foundational equation for estimating pattern width and thickness.

$$a = \frac{\pi R_s^4}{8\mu v_0 h}\left(\frac{dp}{dz}\right) \tag{1}$$

In this equation, a represents the line width pattern, R_s stands for the nozzle tip diameter, μ denotes the ink viscosity, v_0 represents the printing speed, h is the thickness of the printed pattern, and dp/dz signifies the differential of the printing pressure.

One limitation of the current mathematical model is its lack of adaptability across various substrate types, as it does not account for differences in SSE. To address this, improvements to the mathematical model are proposed by integrating SSE, which is crucial for predicting the behavior of conductive ink on diverse surfaces. Incorporating SSE into the model requires a refined focus on the interaction between the deposited conductive ink and the substrate, specifically at the point of deposition. The deposited conductive ink forms a half-spherical cap shape on the substrate [27-28], establishing a simple geometric relationship between the ink and substrate, as illustrated in Fig. 2 (b) and Fig. 2 (c). The variables related to the substrate are defined as follows: R^* represents the radius of the half-spherical cap depicting the conductive ink deposit, a denotes the line width of the conductive ink track, h is the height of the ink track, and θ represents the contact angle of the deposited ink. In this improved mathematical model, SSE is directly related to the contact angle, which is measured using contact angle measurement technique. In this method, a droplet of a known liquid is deposited onto the substrate surface, and the angle formed between the droplet's tangent and the substrate surface is measured [29]. To enhance the model, an equation is proposed that incorporates contact angle, allowing the height of the ink track to be replaced by the contact angle in the previous mathematical model.

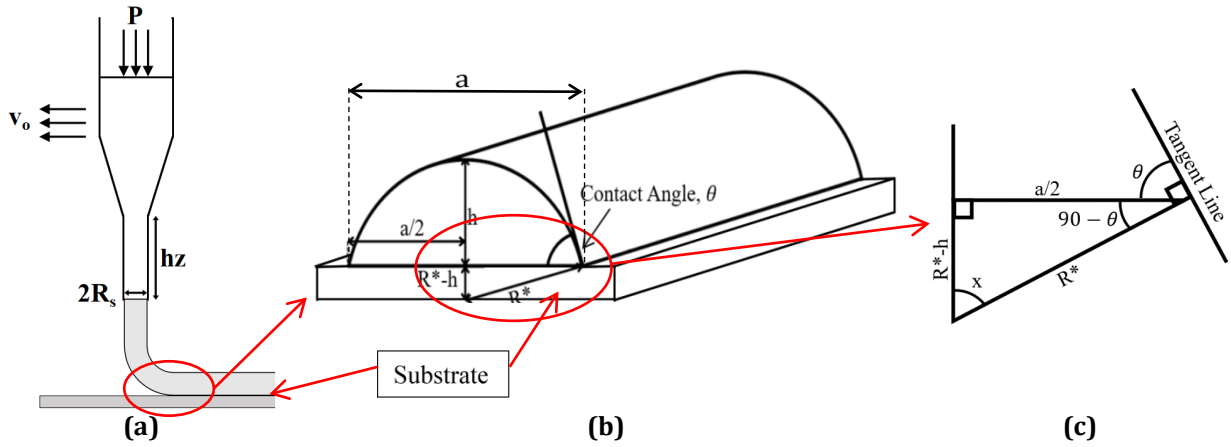

Fig. 2 *A schematic diagram of (a) A representation of printing the ink (at the nozzle tips) on the substrate; (b) Interaction between ink and substrate; (c) A trigonometric representation to determine R**

By applying the formula for a half-spherical cap in conjunction with trigonometric principles, the height of the ink track could be formulated as a function that incorporates the contact angle. Using these trigonometric relationships, along with the schematic diagram presented in Fig. 2(c), Eq. (2) and Eq. (3) are developed.

$$R^* = \frac{a/2}{\sin\theta} \tag{2}$$

$$h = R^*(1 - \cos\theta) \tag{3}$$

The height of the ink track, which incorporates the contact angle, could be formulated by substituting Eq. (2) into Eq. (3). The resulting equation for the height of the ink track is presented in Eq. (4).

$$h = \frac{a}{2}\left(\tan\frac{\theta}{2}\right) \tag{4}$$

The improved mathematical model could be derived by substituting Eq. (4) into the previous mathematical model. This improved mathematical model enables the incorporation of the contact angle variable, which is related to SSE, into the improved mathematical framework, as shown in Eq. (5). The schematic diagram at the nozzle tip is illustrated in Fig. 2(a). Eq. (4) can then be expressed as follows:

$$a = \sqrt{\frac{2\pi {R_s}^4}{8\mu\left(\tan\frac{\theta}{2}\right)v_0}\left(\frac{p}{hz}\right)} \tag{5}$$

where a represents the line width pattern, R_s stands for the nozzle tip diameter, μ denotes the ink viscosity, v_0 represents the printing speed, θ is the contact angle of the deposited ink, P is printing pressure applied and hz signifies the length of nozzle tip. The improved mathematical model could be utilized to predict the line width of conductive ink tracks by incorporating the newly integrated variable of contact angle, which is directly related to SSE. This enhancement means that the improved model is applicable across a range of substrates with varying SSE values, allowing for more versatile and accurate predictions of ink deposition behavior.

2.3 Deposition Process

A syringe-based deposition system, utilizing the FISNAR F4200N machine, was employed for precise application of conductive ink, as shown in Fig. 3(a). This system is specifically designed to enable accurate and controlled ink deposition, ensuring high consistency in results. In this study, two experiments were conducted. The initial

Int. Journal of Integrated Engineering Vol. 17 No. 9 (2025) p. 274-284

experiment applied the previous mathematical model, as shown in Eq. (1), while the second experiment utilized an improved mathematical model that incorporated SSE and ST considerations, as presented in Eq. (5). The printing speed for both experiments was simulated based on the printing pressure and a targeted line width of 0.8 mm.

Optimal printing parameters were determined based on the specifications detailed in Table 1, which served as a guide for achieving the best performance in the printing process. The study utilized an inline curing system to streamline the workflow, where the curing process was integrated directly into the printing setup as shown in Fig. 3(b). A halogen lamp was employed as the heating mechanism for curing, providing efficient and effective thermal management during the curing phase. This approach not only enhanced the overall process efficiency but also improved the quality of the printed conductive ink on the substrate.

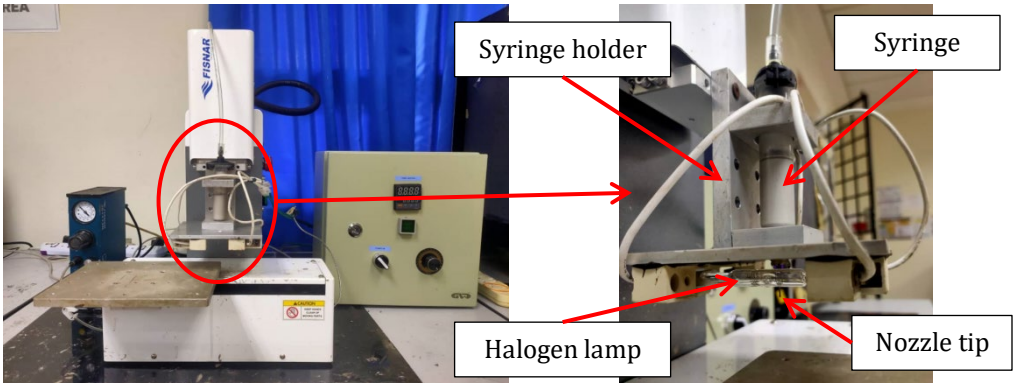

Fig. 3 *(a) Automated syringe deposition machine (Model: Fisnar F4200N); (b) Installed inline curing system*

Table 1 *Printing parameters*

Targeted Line width (mm)	Printing pressure (kPa)	Deposition Height (mm)	Nozzle Diameter (mm)	Conductive Ink Viscosity (Pa.s)
0.80	80/100/120	1.00	0.51	2.40

The morphological analysis of the cured samples was conducted using an optical microscope to obtain magnified images of the silver ink tracks. These images were then analyzed to quantify the line width of the tracks. Measurements were taken at three distinct locations on each sample: the head, middle, and tail. Fig. 4 provides a visual representation of the measurement locations used for calculating the average line width.

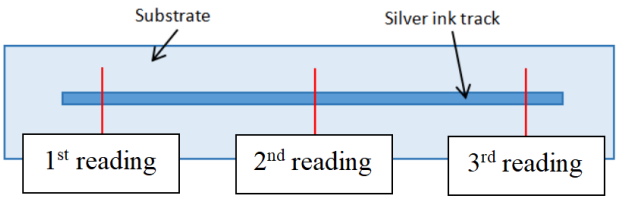

Fig. 4 *Location for measurement taken for average line width*

3. Result and Discussion

The previous mathematical model as presented in Eq. (1), was employed for the initial experiment without incorporating additional variables that may influence the printing process. The simulated printing speeds, derived from this model, are presented in Table 2. Upon reviewing the data in Table 2, it is clear that the printing speed remains relatively low under the conditions tested. However, an increase in printing pressure correlates with a notable enhancement in printing speed. This relationship is further illustrated in Fig. 5, where the positive trend between printing pressure and speed is depicted graphically. This observation is consistent with theoretical principles that dictate the mechanics of printing. Specifically, to achieve targeted line widths in printed electronics, it is imperative to adjust the printing speed in accordance with variations in printing pressure. Increased pressure facilitates greater material flow, necessitating a proportional increase in speed to maintain uniformity and accuracy in the deposited lines [30].

Table 2 *Simulation results based on previous mathematical model*

Run	Constant Perimeter	Input Parameter		Result Parameter
		Printing Speed (mm/s)	Printing Pressure (kPa)	Targeted Line Width (mm)
1	Viscocity = 2.4 Pa.s	0.35	80	0.8
2	Diameter of nozzle tip = 0.51 mm	0.43	100	0.8
3	Thickness of printed pattern = 0.2 mm	0.52	120	0.8

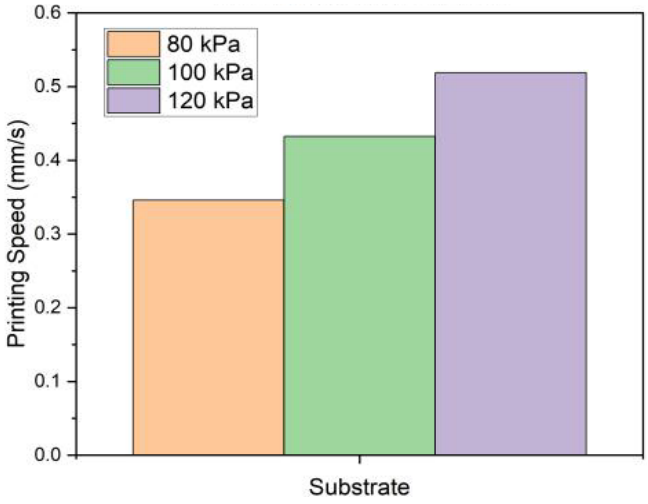

Fig. 5 *The resultant of printing speed across substrates under different applied printing pressures for previous mathematical model*

The initial experiment for ink deposition was conducted using the printing speeds derived from the simulated results. Fig. 6 displays the initial experiment cured samples from this initial experiment. Upon measuring the cured samples, it was observed that the average line width for each sample exceeded 2 mm, resulting in a percentage error of over 150%. The target line width was set at 0.8 mm; thus, the results from the initial experiment significantly surpassed this target. These findings clearly indicate that the previous mathematical model requires refinement. Variables such as SSE and ST, which are critical for the deposition process, need to be integrated into the previous mathematical model. Addressing these factors will enhance the model's accuracy and improve the consistency of the deposition results [16].

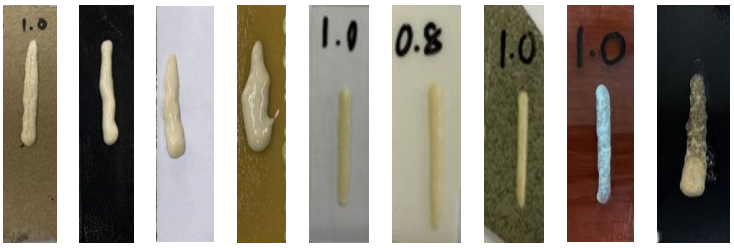

Fig. 6 *Initial experiment cured sample (line width > 2 mm)*

Table 3 presents the simulated printing speeds for the improved mathematical model, calculated using Eq. (5), which incorporates SSE as an additional variable. It is evident that the printing speeds achieved with the improved model are significantly higher compared to those from the initial experiment, ranging between 8.65 mm/s and 83.09 mm/s. This reflects a clear distinction in performance between the two simulations. Fig. 7(a) illustrates the relationship between printing speed and substrates with varying SSE values. Analysis of Fig. 7(a) and Table 3 reveals two main trends: printing speed increases with both rising pressure and higher SSE values.

Int. Journal of Integrated Engineering Vol. 17 No. 9 (2025) p. 274-284

The relationship between printing speed and pressure was previously discussed in the initial experiment. The following analysis emphasizes the influence of SSE in the improved mathematical model on the printing process.

When a substrate exhibits high SSE, the deposited ink adheres more effectively to the substrate's surface, facilitating enhanced adhesion and promoting stronger interaction between the ink and substrate [31]. This improved adhesion is attributed to the increased molecular attraction at the interface, which encourages the ink to spread across the surface more uniformly. As a result, attaining the desired line width often requires a higher printing speed to mitigate the natural tendency of the ink to spread. If printing speed is insufficiently adjusted, the spreading effect may cause the line width to exceed the targeted dimension.

In contrast, substrates with low SSE demonstrate weaker adhesive interactions, resulting in poorer adhesion between the ink and the substrate. This weaker interaction hinders the ink's ability to spread, allowing it to remain more localized upon deposition. As a result, ink on low-SSE substrates typically retains its initial placement, with minimal spread, thereby maintaining a more controlled line width [32]. Thus, to achieve consistent, targeted line widths across varying SSE substrates, careful tuning of printing speed is essential. High-SSE substrates require greater speed adjustments to counteract spreading, while low-SSE substrates benefit from lower speeds, as the ink remains more contained upon deposition.

Table 3 *Simulation and experimental results based on improved mathematical model*

Run	Categories	Substrate	Contact angle (°)	SSE (mJ/m^2)	Input Parameter		Result Parameter		
					Printing Speed (mm/s)	Printing Pressure (kPa)	Average Line Width (mm)	Targeted Line Width (mm)	Percentage Error (%)
1	Low	Cardboard	115.23	16.80	8.65	80	0.72	0.80	10.25
2					10.82	100	0.73	0.80	8.30
3					12.98	120	0.77	0.80	4.25
4		Leather	111.95	18.14	9.19	80	0.74	0.80	7.35
5					11.49	100	0.79	0.80	1.51
6					13.79	120	0.81	0.80	0.86
7		Rubber dye fabric	100.08	24.87	11.41	80	0.79	0.80	1.29
8					14.27	100	0.81	0.80	0.65
9					17.12	120	0.81	0.80	1.65
10	Medium	FR4	73.98	40.55	18.08	80	0.81	0.80	0.81
11					22.60	100	0.82	0.80	2.81
12					27.12	120	0.84	0.80	5.02
13		Glass	67.01	44.79	20.57	80	0.83	0.80	3.76
14					25.71	100	0.83	0.80	3.39
15					30.85	120	0.84	0.80	4.66
16		Porcelain	64.43	46.35	21.61	80	0.82	0.80	3.08
17					27.02	100	0.84	0.80	5.03
18					32.42	120	0.86	0.80	7.24
19	High	Unglazed ceramic tile	55.48	51.60	25.90	80	0.86	0.80	7.80
20					32.37	100	0.90	0.80	12.32
21					38.85	120	0.92	0.80	15.35
22		Polyimide	41.27	59.24	36.17	80	0.83	0.80	4.24
23					45.21	100	0.84	0.80	4.76
24					54.25	120	0.85	0.80	5.87
25		Ceramic tile	27.63	65.39	55.40	80	0.91	0.80	13.61
26					69.24	100	0.91	0.80	14.14
27					83.09	120	0.93	0.80	15.82

The second experiment employed the printing speeds simulated in Table 3, with line width measurements taken at three different points for each cured sample to ensure accurate averaging. Table 3 summarizes the average line width and corresponding percentage error for samples produced using the improved mathematical model. Fig. 7(b) illustrates the relationship between average line width and substrate type, while Fig. 7(c) presents the percentage error in line width across various substrates. Additionally, Fig. 8 includes example of morphological images of the cured samples, which were utilized to accurately measure line width and assess the uniformity of ink deposition across different substrate surfaces. The results in Table 3 show that line widths achieved with the improved model range between 0.72 mm and 0.92 mm, which represents a significant improvement over the initial experiment, where line widths exceeded 2 mm. This improvement is largely attributed to the incorporation of SSE into the mathematical model, enabling a better balance between ink flow and adhesion [20]. Higher SSE values increase ink spread, requiring higher printing speeds to control line width, which aligns well with the observed improvement in accuracy [30].

Furthermore, the results reveal that the average line width tends to increase with the SSE of the substrate. High-SSE substrates enhance ink adhesion and spreading, resulting in wider lines if printing speed adjustments are not precisely calibrated. This relationship underscores the importance of incorporating substrate-specific properties, like SSE, into the model to achieve targeted line widths reliably across diverse substrate types. The percentage error in line width measurement, as shown in Table 3, also reflects significant improvements. The percentage error ranges from 0.81% to 15.82%, indicating enhanced consistency in line width. As illustrated in Fig. 7(c), substrates with high SSE exhibit the highest percentage error, likely due to the increased variability in ink spreading caused by strong adhesion forces. This effect necessitates careful control over printing speed, particularly for high-SSE substrates, to mitigate spreading and achieve consistent line widths.

Notably, despite cardboard having a low SSE, it exhibits a relatively high percentage error. This anomaly attributed to the absorbent nature of cardboard, which causes the conductive ink to be partially absorbed into the substrate, thinning the ink layer and resulting in unpredictable line widths [33-34]. This finding emphasizes that while SSE is a key factor, substrate porosity and absorbency must also be considered in future model adjustments, particularly for porous materials like cardboard, where ink spread and consistency may be affected by absorption.

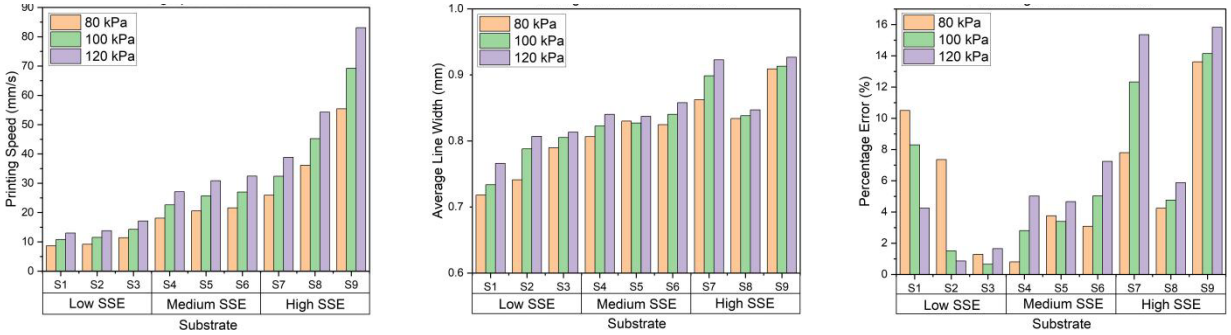

Fig. 7 *Experimental results obtained using the improved mathematical model (a) Printing speed across various substrates with different SSE under different applied printing pressures; (b) Average line width was measured across various substrates with different SSE under different applied printing pressures; (c) Percentage error in the average line width was evaluated across various substrates with different SSE under different applied printing pressures, with a targeted line width of 0.8 mm*

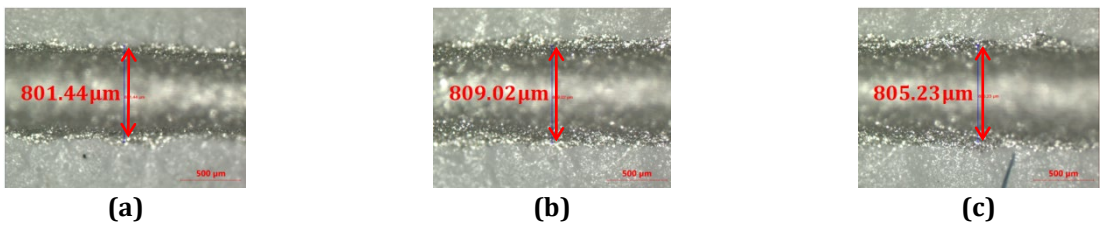

Fig. 8 *Image of determination of average line width measurement (a) First reading (head); (b) Second reading (middle); (c) Third reading (tail)*

4. Conclusion and Recommendations

This study demonstrates that integrating SSE and ST into previous mathematical model significantly enhances the precision of ink track width estimation in conductive ink printing. The addition of SSE and ST enables more accurate adjustments to printing parameters, leading to improved process control and uniformity across diverse substrates. Initial experiments using previous mathematical model showed significant discrepancies, with line widths exceeding 2 mm and percentage errors surpassing 150%. In contrast, the improved model achieved line widths between 0.72 mm and 0.92 mm, with the highest percentage error reduced to 15.82%. This improvement highlights the importance of SSE in controlling line width, as high-SSE substrates encourage ink spreading, necessitating higher printing speeds for precision, while low-SSE substrates allow ink to remain more localized. Notably, substrates like cardboard, with low SSE but high porosity, exhibited relatively high errors due to absorbency, emphasizing the need to consider both substrate porosity and SSE for accurate deposition predictions.

Based on these findings, several recommendations are proposed to further enhance ink deposition accuracy. Future models should incorporate substrate porosity and absorbency, as absorbent materials significantly impact deposition consistency. Additionally, employing a specific simulation tool can provide deeper insights into ink behaviour during deposition, aiding in the optimization of deposition parameters via controlling the dispersion rate of the ink. Adjusting ink viscosity to counteract the challenges posed by high-SSE substrates is also recommended, as controlling viscosity can reduce excessive ink spread and improve line precision. Optimizing printing speed for high-SSE surfaces remains crucial, as these surfaces increase ink spread and require precise speed adjustments for controlled line width. Developing a database of substrate-specific printing parameters based on SSE, porosity, and viscosity could streamline industrial processes, making the model more versatile and practical. Expanding the model's application to various conductive inks would further validate its utility in diverse printed electronics applications. Additionally, refining the mathematical model to incorporate these factors will enhance its predictive accuracy. Finally, improving inline curing systems is advised, as this could boost deposition quality and efficiency, especially in high-throughput manufacturing. These enhancements aim to improve the accuracy, consistency, and adaptability of conductive ink deposition across different substrates, supporting advancements in printed electronics and flexible device production.

Acknowledgement

This research was supported by Ministry of Higher Education (MOHE) through Fundamental Research Grant Scheme (FRGS/1/2023/TK10/UTHM/02/12) and Universiti Tun Hussein Onn Malaysia through GPPS (vot Q581) and Tier 1 (vot Q357).

References

[1] Masripan, N., Jin, L., Salim, M. A., Abdul Hamid, N., Mansor, M. R., Akop, M. Z., ... & Wasbari, F. (2021). Effect of stretchable conductive ink (SCI) on electrical conductivity under tensile stress. International Journal of Nanoelectronics and Materials, 14, 429-438, http://dspace.unimap.edu.my/xmlui/handle/123456789/73443

[2] Salim, M. A., Saad, H., Ali, M., Dai, F., Saad, A. M., Masripan, N. A., & Wasbari, F. (2022). Effect on Electrical Conductivity of Graphene Nanoparticle Filled Epoxy Conductive Ink. Encyclopedia of Smart Materials, 3, 109-118, https://doi.org/10.1016/b978-0-12-815732-9.00155-8

[3] Li, L. H., Mo, L. X., Ran, J., & Xin, Z. (2014). Conductive ink and its application technology progress. Imaging Science and Photochemistry, 32, 393-401, http://dx.doi.org/10.7517/j.issn.1674-0475.2014.04.393

[4] Wang, H., Wang, B., & Ning, X. (2021). Research progress in conductive inks for inkjet printing and its application for intelligent electronic textiles. Journal of Textile Research, 42(6), 189-197. https://doi.org/10.13475/j.fzxb.20200701809

[5] Phillips, C., Al-Ahmadi, A., Potts, S. J., Claypole, T., & Deganello, D. (2017). The effect of graphite and carbon black ratios on conductive ink performance. Journal of Materials Science, 52(16), 9520-9530. https://doi.org/10.1007/s10853-017-1114-6

[6] Yang-Pei-Qi Yi, Y. L. (2019). Inkjet conductive inks for printing textile materials and applications. Journal of Fiber Bioengineering and Informatics, 12(1), 11-24. https://doi.org/10.3993/jfbim00310

[7] Hoskins, C., Zukova, A., Turnblade, J., Shi, Y., Burolla, S. (2016) Inkjet printed antennas. Proceedings of the International Telemetering Conference, 52, 537-548, http://hdl.handle.net/10150/624234

[8] Shabbir, M. K., Syed, A. S., & Akhtar, J. (2023). Smart multifunctional polymeric inks for supercapacitor applications. In Smart Multifunctional Nano-inks (pp. 429-449). Elsevier. https://doi.org/10.1016/b978-0-323-91145-0.00028-1

[9] Lee, H. U., Jin, J. H., & Chung, B. G. (2022). High-capacity three-dimensional solar rechargeable micro-supercapacitor using MnO2/V2O5-based binary metal oxide nanocomposite ink. Journal of Industrial and Engineering Chemistry, 115, 544-553, https://doi.org/10.1016/j.jiec.2022.08.042

[10] Yan, H., Cai, W., Zhang, Y., Wang, H., & Liu, Y. (2017). Review of conductive inks in printed electronics. Journal of Beijing University of Technology, 43(7), 1117-1122, http://dx.doi.org/10.11936/bjutxb2017010028

[11] Vozzi, G., Previti, A., De Rossi, D., & Ahluwalia, A. R. T. I. (2002). Microsyringe-based deposition of two-dimensional and three-dimensional polymer scaffolds with a well-defined geometry for application to tissue engineering. Tissue engineering, 8(6), 1089-1098, https://doi.org/10.1089/107632702320934182

[12] Zainal, M. N., Khirotdin, R. K., Eraman, S. N. E., Suhaimi, M. F. N., & Hassan, N. (2022). Investigation of Curing Process of Silver Conductive Ink on Polymer Substrates Using Halogen Lamp and Oven. Technological Advancement in Instrumentation & Human Engineering: Selected papers from ICMER 2021, 882, 387, https://doi.org/10.1007/978-981-19-1577-2_29

[13] Aydemir, C., Altay, B. N., & Akyol, M. (2021). Surface analysis of polymer films for wettability and ink adhesion. Color Research & Application, 46(2), 489-499, https://doi.org/10.1002/col.22579

[14] Cinquino, M., Prontera, C. T., Zizzari, A., Giuri, A., Pugliese, M., Giannuzzi, R., Monteduro, A. G., Carugati, M., Banfi, A., Carallo, S., Rizzo, A., Andretta, A., Dugnani, G., Gigli, G., & Maiorano, V. (2022). Effect of surface tension and drying time on inkjet-printed PEDOT: PSS for ITO-free OLED devices. Journal of Science: Advanced Materials Devices, 7(1), 100394, https://doi.org/10.1016/j.jsamd.2021.09.001

[15] Lee, H. H., Chou, K. S., & Huang, K. C. (2005). Inkjet printing of nanosized silver colloids. Nanotechnology, 16(10), 2436, https://doi.org/10.1088/0957-4484/16/10/074

[16] Matavž, A., Bobnar, V., & Malič, B. (2017). Tailoring ink–substrate interactions via thin polymeric layers for high-resolution printing. Langmuir, 33(43), 11893-11900, https://doi.org/10.1021/acs.langmuir.7b02181

[17] Joyce, M., Pal, L., Hicks, R., Agate, S., Williams, T. S., Ray, G., & Fleming, P. D. (2018). Custom tailoring of conductive ink/substrate properties for increased thin film deposition of poly (dimethylsiloxane) films. Journal of Materials Science: Materials in Electronics, 29, 10461-10470, https://doi.org/10.1007/s10854-018-9108-y

[18] Yuan, Z., Matsumoto, M., & Kurose, R. (2021). Stability of the non-wetting state in a droplet impinging on surfaces with multiple holes. Physics of Fluids, 33(12), https://doi.org/10.1063/5.0071333

[19] Wen, X., Wang, L., & Deng, W. (2019). Study on preparation and stability of acrylic resin based waterborne pigment marker ink. China Surfactant Deterg Cosmet, 49(3), 167-173, https://doi.org/10.3969/j.issn.1001-1803.2019.03.006

[20] Mikkonen, R., & Mäntysalo, M. (2018). Evaluation of screen printed silver trace performance and long-term reliability against environmental stress on a low surface energy substrate. Microelectronics Reliability, 86, 54-65, https://doi.org/10.1016/j.microrel.2018.05.010

[21] Mendez-Rossal, H. R., & Wallner, G. M. (2019). Printability and Properties of Conductive Inks on Primer-Coated Surfaces. International Journal of Polymer Science, 2019(1), 3874181, https://doi.org/10.1155/2019/3874181

[22] Vafaei, S., Tuck, C., Wildman, R., & Ashcroft, I. (2016). Spreading of the nanofluid triple line in ink jet printed electronics tracks. Additive Manufacturing, 11, 77-84. https://doi.org/10.1016/j.addma.2016.04.005

[23] Mallinson, S. G., McBain, G. D., & Horrocks, G. D. (2016, December). Viscosity and surface tension of aqueous mixtures. In 20th Australasian Fluid Mechanics Conference Perth, Australia. Australasian Fluid Mechanics Society. https://www.researchgate.net/publication/309286803

[24] Ali, M., Lin, L., Faisal, S., Sahito, I. A., & Ali, S. I. (2019). Optimisation of screen printing process for functional printing. Pigment & Resin Technology, 48(5), 456-463, https://doi.org/10.1108/PRT-05-2019-0043

[25] Hou, X., Chen, G., & Xing, T. (2020). Influence of physical property of reactive ink fluid on jetting behaviour. Journal of Textile Research, 41(3), 91-99, https://doi.org/10.13475/j.fzxb.20190501809

[26] Qu, Z., Liu, S., Wei, Q., & Zhang, Y. (2015). Research on the performance of screen printing line in water conductive ink. In Advanced Graphic Communications, Packaging Technology and Materials (pp. 477-482). Singapore: Springer Singapore. https://doi.org/10.1007/978-981-10-0072-0_60

[27] Khirotdin, R. K., Zainuri, M. I. S. M., Ishak, A. I., Hassan, N., Kamarudin, K., Ibrahim, M. R., Abdul Haq, R. H., Ibrahim, M., Sau'de, N., & Marwah, O. M. F. (2017). Printing and curing of conductive ink track on fabric using syringe deposition system with dlp projector and hot plate. In MATEC Web of Conferences (Vol. 135, p. 00047). EDP Sciences. https://doi.org/10.1051/matecconf/201713500047

[28] Khirotdin, R. K., Nazli, M. M. M. N., Mahadzir, M. A., & Hassan, N. (2019). Printing and curing of conductive inks on fabric using syringe-based deposition system and oven for wearable antenna application. In Journal of Physics: Conference Series (Vol. 1150, No. 1, p. 012039). IOP Publishing. https://doi.org/10.1088/1742-6596/1150/1/012039

[29] Giridhar, G., Manepalli, R. K. N. R., & Apparao, G. (2017). Contact angle measurement techniques for nanomaterials. In Thermal and rheological measurement techniques for nanomaterials characterization (pp. 173-195). Elsevier. https://doi.org/10.1016/B978-0-323-46139-9.00008-6

[30] Nair, S., Panda, S., Tripathi, A., & Neithalath, N. (2021). Relating print velocity and extrusion characteristics of 3D-printable cementitious binders: Implications towards testing methods. Additive Manufacturing, 46, 102127, https://doi.org/10.1016/j.addma.2021.102127

[31] Madeira, D. M., Vieira, O., Pinheiro, L. A., & de Melo Carvalho, B. (2018). Correlation between surface energy and adhesion force of polyethylene/paperboard: a predictive tool for quality control in laminated packaging. International Journal of Chemical Engineering, 2018(1), 2709037, http://dx.doi.org/10.1155/2018/2709037

[32] Naghieh, S., & Chen, X. (2021). Printability–A key issue in extrusion-based bioprinting. Journal of pharmaceutical analysis, 11(5), 564-579, https://doi.org/10.1016/j.jpha.2021.02.001

[33] Kang, D. J., Gonzaléz-García, L., & Kraus, T. (2022). Soft electronics by inkjet printing metal inks on porous substrates. Flexible and Printed Electronics, 7(3), 033001, https://doi.org/10.1088/2058-8585/ac8360

[34] Jansson, E., Lyytikäinen, J., Tanninen, P., Eiroma, K., Leminen, V., Immonen, K., & Hakola, L. (2022). Suitability of paper-based substrates for printed electronics. Materials, 15(3), 957, https://doi.org/10.3390/ma15030957